Inorganic Chemistry
Cite This: Inorg. Chem. 2018, 57, 5299−5306
Article
pubs.acs.org/IC

Solvent Effects on Growth, Crystallinity, and Surface Bonding of Ge Nanoparticles

Andrew Bernard,[†] Keye Zhang,[†] Daniel Larson,[†] Katayoon Tabatabaei, and Susan M. Kauzlarich*[†]

Department of Chemistry, University of California, One Shields Avenue, Davis, California 95616, United States

Supporting Information

ABSTRACT: Solvent effects on the microwave-assisted synthesis of germanium nanoparticles are presented. A mixture of oleylamine and 1-dodecene was used as the reaction solvent. Oleylamine serves as a reducing agent in the synthesis while both molecules act as binding ligands. Increased concentrations of 1-dodecene in the solvent mixture were found to increase the size of the formed nanoparticles. Crystallinity was also dependent on the solvent mixture. Amorphous nanoparticles were obtained at lower 1-dodecene concentrations, whereas, at higher concentrations, particles contained crystalline and amorphous domains. 11-Methoxyundec-1-ene was synthesized to replace 1-dodecene in the reaction mixture for nuclear magnetic resonance (NMR) studies. ^{1}H NMR of the reaction products shows that both solvent molecules in the system act as binding ligands on the nanoparticle surface. Nanoparticles were characterized using powder X-ray diffraction, scanning transmission electron microscopy, and spectroscopy techniques (Raman, UV−vis, FT-IR, and NMR).

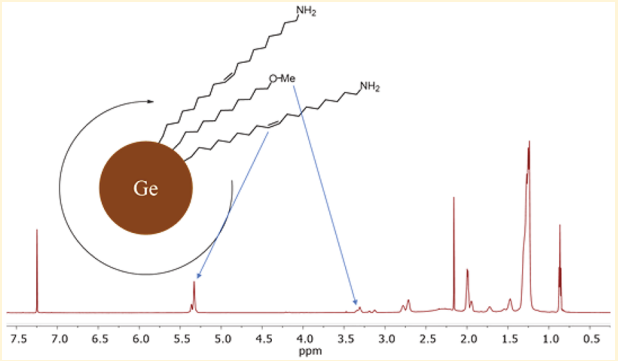

INTRODUCTION

Ge nanoparticles (NPs) have been of interest for several years due to their applications in optoelectronics, bioimaging, batteries, and solar energy conversion.[1−5] The element Ge has several traits that make it useful as a nanoscale semiconductor. Compared to Si, Ge has a superior absorption coefficient and charge transport capabilities. It also has a bulk band gap of 0.67 eV at 300 K (Si E_g = 1.11 eV at 300 K), which can be tuned through size control due to quantum confinement effects.[6]

A variety of methods to prepare colloidal Ge NPs have been studied, including the thermal decomposition of organogermane single-source precursors,[7] metathesis of Ge Zintl phases,[8−11] reduction of Ge halides using mild to strong reductants,[4,12−14] reduction of GeO_2 powders,[15,16] and microwave-assisted reduction of GeI_2 in organic media.[17] These methods involve high temperatures and pressures,[18] intricate or time-consuming Ge precursor syntheses,[10,11] and pyrophoric or flammable reducing agents.[4,12−14] For reactions involving Ge halides, known variables that effect the morphology of the produced Ge NPs include: strength of the reducing agent, temperature, and solvent.[19] Due to Ge's crystallization temperature (~450 °C), high temperature is typically required for the formation of Ge nanocrystals.[17,20,21] This also means that solvents with a high boiling point, or solvents at supercritical conditions are usually necessary to synthesize nanocrystalline Ge.[18] Crystalline Ge NPs have been made at room temperature using strong reducing agents such as $LiAlH_4$, *n*-butyllithium, and *tert*-butyllithium.[4,22]

Although there is significant interest in nanocrystalline Ge, amorphous Ge is also of interest. Ge possesses a high Li-ion diffusion coefficient and theoretical capacity (1600 mAh/g), which makes it an attractive material for a battery anode. However, bulk Ge suffers a large volume change that compromises the material's structure during the Li-Ge alloying−dealloying process, which slowly cripples the cyclability of a Ge anode. Amorphous Ge nanowires have been shown to retain high capacity after hundreds of cycles.[23] Also, hollow amorphous Ge nanostructures are expected to help alleviate problems with strain during the Li alloying−dealloying process.[24,25]

Alkyl-capped Ge nanocrystals have been shown to exhibit photoluminescence in the visible and near-infrared regions.[4,9,10,26,27] Photoluminescent NPs find applications in light-emitting diodes, solar cells, and as biolabels. However, toxicity concerns over the use of metals such as lead, cadmium, and mercury in common photoluminescent NPs have been raised, making Ge NPs an attractive alternative.[28,29] Ge NPs exhibiting photoluminescence have been fabricated using both physical[30,31] and colloidal[4,11,27] methods. The physical approaches produce matrix or substrate-bound particles, making these processes too expensive or unscalable, limiting their potential applications. Colloidal methods for synthesizing near-IR emitting Ge NPs typically involve hot injection of a strong reducing agent such as *n*-BuLi or $LiAlH_4$ in primary

Received: February 5, 2018
Published: April 19, 2018

DOI: 10.1021/acs.inorgchem.8b00334
Inorg. Chem. 2018, 57, 5299−5306

alkene to a solution of GeI_2 in oleylamine or hexadecylamine. The long chain amines act as a solvent to dissolve the Ge precursor; these two reducing agents are thought to put hydrogen on the surface so the primary alkene can act as the capping ligand by means of hydrogermylation once the Ge has been reduced.[4,27,32] While the nanocrystals prepared by this route provide near-IR photoluminescence as made, upon exposure to an ambient atmosphere, the spectrum degrades and either they totally lose their photoluminescence or else a blue shift to the visible region is observed.[4] The loss of photoluminescence indicates that better surface passivation is necessary for these NPs to retain their photoluminescent properties and to be feasible for applications that require near-IR emission.

Finding a colloidal method to produce near-IR emitting Ge NPs using a simple reduction of GeI_2 without the presence of strong reducing agents would be beneficial for further research and upscaling. Solvent effects on crystallinity, shape, and size have already been explored for other NP systems including $MnFe_2O_4$,[33] ZnSe,[34] and Co[35] but not for Ge NPs. The aim of this work is two-fold: to find a simple route to alkyl-capped Ge NPs via microwave synthesis, and to investigate the effect solvent has on the surface structure and growth of Ge NPs.

EXPERIMENTAL SECTION

Materials. GeI_2 was provided by Prof. Richard Blair's laboratory (University of Central Florida).[36] Oleylamine (OAm, 40%), purchased from TCI, and 1-Dodecene (DDE, 95%), purchased from Sigma-Aldrich, were dried and degassed by heating them under vacuum at 125 °C for an hour, followed by an argon purge for 45 min. 11-Bromo-1-undecene (95%), potassium hydroxide (KOH, 85%), methanol (99.8%, anhydrous), and diethyl ether (99%) were purchased from Sigma-Aldrich. Anhydrous magnesium sulfate (powder/certified) was purchased from Fisher Scientific. Toluene (99.9%, HPLC) was purchased from Sigma-Aldrich and dried by passing it over two activated alumina columns under nitrogen.

Synthesis of Alkyl/Oleylamine Capped Ge Nanoparticles. Ge NPs were synthesized in a CEM Discover microwave reactor under an argon atmosphere. In an argon-filled drybox, 130.6 mg of GeI_2 (0.4 mmol) was added to a degassed solution of OAm and either DDE or 11-methoxyundec-1-ene (MUE) with a total volume of 8 mL in a 35 mL CEM reaction vessel, capped to protect from moisture and removed. The GeI_2 was fully dissolved by sonicating for 20 min. Primary alkene quantities ranged from 0% to 50% of the total solvent volume. The resulting solution was heated and stirred in the microwave at 240 °C for 1 h on dynamic mode with a maximum power of 300 W. After heating, the dark brown solution was then transferred to a centrifuge tube. The NPs were isolated using a solvent–antisolvent mixture of 2 mL of dried toluene and 30 mL of anhydrous methanol. The resulting mixture was centrifuged at 8500 rpm for 30 min. After each centrifugation, the solvent was decanted to isolate the NPs. This process was repeated twice. After the final centrifugation, the isolated NPs were stored under 5 mL of toluene in an argon-filled drybox to await further analysis.

Synthesis of 11-Methoxyundec-1-ene from 11-Bromoundec-1-ene. The synthesis of 11-methoxyundec-1-ene was adapted from a literature procedure.[37] Under air, anhydrous methanol (55 mL) in a 250 mL round-bottom flask was cooled to 0 °C in an ice bath. KOH (96 mmol, 5.035 g) was added to the cooled methanol and stirred until dissolved (~30 min). A solution of 11-bromoundec-1-ene (7.5 mL, 7.97g) in anhydrous methanol (65 mL) was added dropwise to the KOH–methanol solution, and the mixture was refluxed at 70 °C overnight. The methanol was removed *in vacuo*, and the crude mixture was neutralized with 50 mL of 2 M HCl and diluted with 10 mL of anhydrous diethyl ether. The crude product was extracted using diethyl ether (4 × 50 mL). The combined organic layers were dried with anhydrous magnesium sulfate and concentrated *in vacuo* to yield a colorless oil (5.86g, 93%): ^{1}H NMR (400 MHz, C_6D_6) δ 5.80 (ddt, J = 16.9, 10.2, 6.7 Hz, 1H), 5.10–4.95 (m, 2H), 3.23 (t, J = 6.5 Hz, 2H), 3.15 (s, 3H), 2.04–1.94 (m, 2H), 1.61–1.51 (m, 2H), 1.39–1.20 (m, 12H) ; ^{13}C NMR (101 MHz, C_6D_6) δ 138.9, 114.1, 72.6, 57.9, 33.9, 29.8, 29.6, 29.5, 29.5, 29.2, 29.0, 26.3.

Characterization. Powder X-ray diffraction (PXRD) was performed on a Bruker D8 Advance diffractometer with Cu Kα lines (40 kV, 40 mA). PXRD samples were prepared by evaporating a small amount of the Ge NP dispersion on a quartz holder. The data were acquired in the 2θ range of 20–80°. Crystallite size estimations of the NPs were obtained by fitting the {220} reflection (Pseudo-Voigt) using Jade 5.0 software. Scanning transmission electron microscopy (STEM) was performed using a Schottky emitter (Model JEOL JEM 2100F-AC) electron microscope operated at a voltage of 200 kV. Images were captured using Digital Micrograph software from Gatan, Inc. STEM samples were prepared by placing a drop of diluted Ge NP toluene dispersion on a lacey carbon coated by a 400 mesh Cu grid obtained from Ted Pella. FT-IR spectra were taken on a Bruker Alpha spectrophotometer using an ATR accessory. Under ambient conditions, a drop of the NP suspension was dried on the ATR crystal before collecting its spectrum. Raman spectra were taken using a Reinshaw RM1000 laser Raman microscope (514 nm) with a motorized stage. The Raman laser had an output excitation power of 25 mW attenuated by a 10% neutral density filter. The Raman microscope was calibrated by centering the Si signal of a crystalline Si standard at 520.3 cm^{-1}. Samples were prepared by depositing a Ge NPs solution on aluminum foil, followed by drying the NP dispersion in air. Ultraviolet–visible (UV–vis) spectra of diluted Ge NPs were taken at room temperature on a PerkinElmer Model Lambda 750 spectrophotometer. NMR spectra were collected using a 400 MHz Bruker Avance IIIHD Nanobay and 600 MHz Varian VNMRS spectrometers. NMR samples were prepared by taking 1 mL of the NP suspension, evaporating off the toluene in vacuo, and redispersing in 0.5 mL of $CDCl_3$.

RESULTS AND DISCUSSION

We present the details of a synthetic study to determine whether a primary alkene can react and cap the surface of Ge

Chart 1. Line-Angle Structures of the Ligands DDE, MUE, and OAm

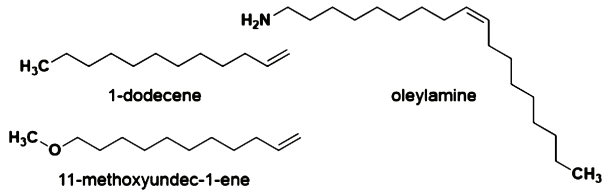

NPs formed in a microwave-assisted reaction in the solvent, oleylamine (OAm). Primary alkenes used in this study were 1-dodecene (DDE) and 11-methoxyundec-1-ene. The structures for the ligands used are shown in Chart 1. Initially, a test reaction of GeI_2 in 100% DDE was run at 210 °C for 1 h to determine whether a reaction could occur between DDE and GeI_2. This reaction showed no color change after heating in the microwave reactor. GeI_2 in OAm under the same conditions forms a dark brown solution from which Ge NPs can be precipitated. Therefore, the results indicated that GeI_2 does not react with DDE and that no Ge NPs are formed from microwave heating of the mixture. This is to be expected, as DDE does not have any reducing ability, whereas OAm has been shown to be a mild reducing agent for many elements to form NPs.[38]

PXRD of the Ge NPs synthesized in the OAm-DDE mixtures shows a featureless pattern indicating an amorphous product

DOI: 10.1021/acs.inorgchem.8b00334
Inorg. Chem. 2018, 57, 5299–5306

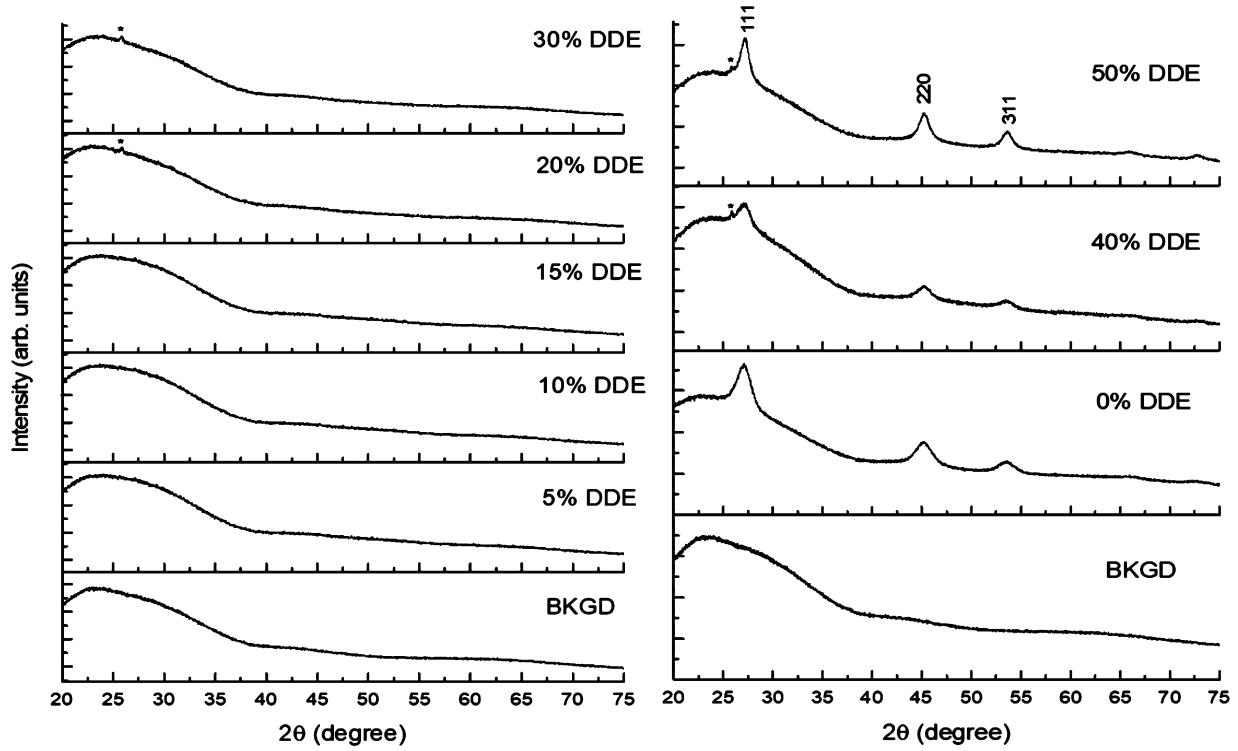

Figure 1. PXRD of DDE/OAm capped Ge NPs. * denotes the (101) reflection of GeO_2.

Table 1. Sizes of DDE/OAm Capped Ge NPs

%DDC	Crystalline	Crys. size (nm)	STEM size[a] (nm)	Bandgap (eV)[b]
50	Yes	6.7±0.3	10.8±3.0	1.09
40	Yes	4.8±0.1	9.5±2.3	1.22
30	No	N/A	6.4±1.6	1.27
20	No	N/A	5.0±1.1	1.28
15	No	N/A	4.6±0.9	1.35
10	No	N/A	5.3±1.2	1.36
5	No	N/A	6.2±1.4	1.29
0	Yes	4.6±0.1	7.5±1.9	1.22

[a]Obtained by analysis of 200 particles per sample. [b]Obtained by Tauc analysis.

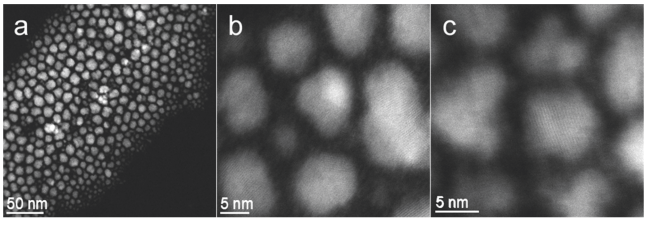

Figure 2. STEM images of (a) Ge NPs made in 50% DDE showing a *quasi*-spherical shape, (b) Ge NPs made in 50% DDE showing lattice fringes, and (c) Ge NPs made in 40% DDE showing lattice fringes.

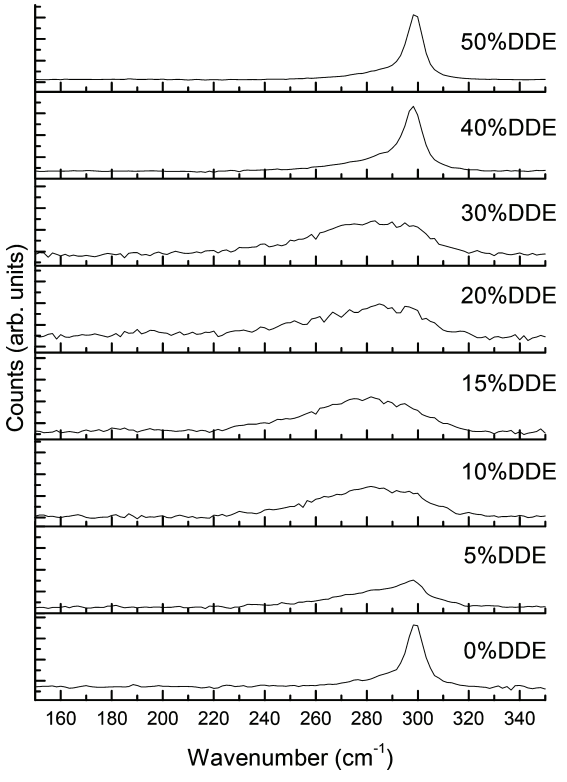

Figure 3. Raman spectra of DDE/OAm capped Ge NPs.

was formed when the concentration of DDE was more than 0% and less than 40% of the total reaction volume (Figure 1). There is a small peak corresponding to GeO_2 in a few of the diffraction patterns and may arise from small amounts of water or oxygen in the solvent mixture during NP isolation. This possibility is consistent with the lack of a Ge-O stretch in the FT-IR spectra for these samples (see discussion below). Ge NPs made in pure OAm are crystalline, as expected from previous literature reports.[17] At 40% and 50% DDE, PXRD shows that crystalline Ge NPs were obtained. Analysis of the

DOI: 10.1021/acs.inorgchem.8b00334
Inorg. Chem. 2018, 57, 5299−5306

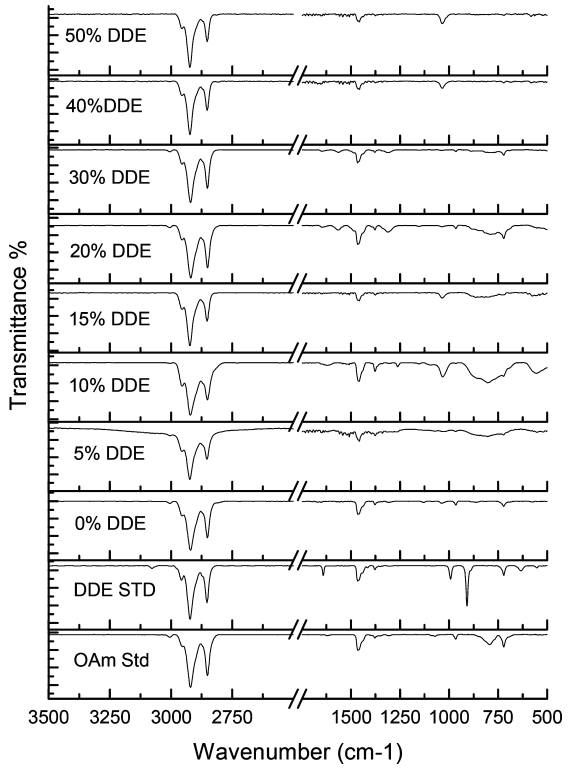

Figure 4. FT-IR spectra of DDE/OAm capped Ge NPs.

{220} reflection in the crystalline Ge NPs allows for the crystallite size to be estimated using the Scherrer equation (Table 1). However, due to the lack of an X-ray diffraction pattern for the Ge NPs made in DDE solutions below 40%, STEM imaging was needed to infer more about the size dependency on the DDE/OAm solvent ratio.

STEM images of the formed Ge NPs showed that particles are *quasi*-spherical (Figure 2a). Histograms were produced to show the average sizes of the Ge NPs by measuring 200 particles per sample (SI, Figures S1−S8). Table 1 shows the particle size determined by both PXRD and STEM images. OAm capped Ge NPs show a particle size of 4.6 ± 0.1 nm from diffraction and 7.5 ± 1.9 nm from STEM. This is consistent with previous publications for Ge NPs prepared from a microwave-assisted process.[17,39] In addition, high temperature solution approaches also show a discrepancy between PXRD and TEM analysis.[4] Initially, increasing DDE concentration decreased particle size until 20% DDE when average size increased (see Table 1). The Ge NPs made in 15% DDE had the smallest average particle size at 4.6 ± 0.9 nm, whereas those made in 50% DDE had the largest size at 10.8 ± 3.0 nm. STEM of the Ge NPs formed in the 40% and 50% DDE solutions show the presence of lattice fringes (Figure 2b,c), which indicate that the particles are crystalline, consistent with the results of PXRD which show a diffraction pattern. For the crystalline Ge NPs prepared with DDE added to the solution, the average particle size from the STEM measurements varied significantly from the average crystallite size from PXRD found using the Scherrer equation. For 50% DDE, the Ge NPs measured 6.7 ± 0.3 nm by PXRD and 10.8 ± 3.0 nm by STEM, whereas the 40% DDE Ge NPs measured 4.8 ± 0.1 nm by PXRD and 9.5 ± 2.3 nm by STEM. The size discrepancy could be due to a mix of amorphous and crystalline NPs, crystalline core−amorphous shell NPs, NPs with crystalline and amorphous regions, or polycrystalline NPs. As can been seen in the case of the amorphous samples (Supporting Information (SI)), there is little contrast in STEM and no lattice fringes are observed. For small amounts of DDE, the particles look spherical; as the amount of DDE increases (>30%), size and shape control is lost. At 40% and higher, crystallinity is apparent from lattice fringes and the particles become *quasi*-spherical when the DDE is at 50% in Figure 2. At 40% DDE, each particle seems to be formed from several particles, supporting the idea that the size discrepancy between the two measurements could be attributed to polycrystalline NPs or a more complex amorphous−crystalline scenario.

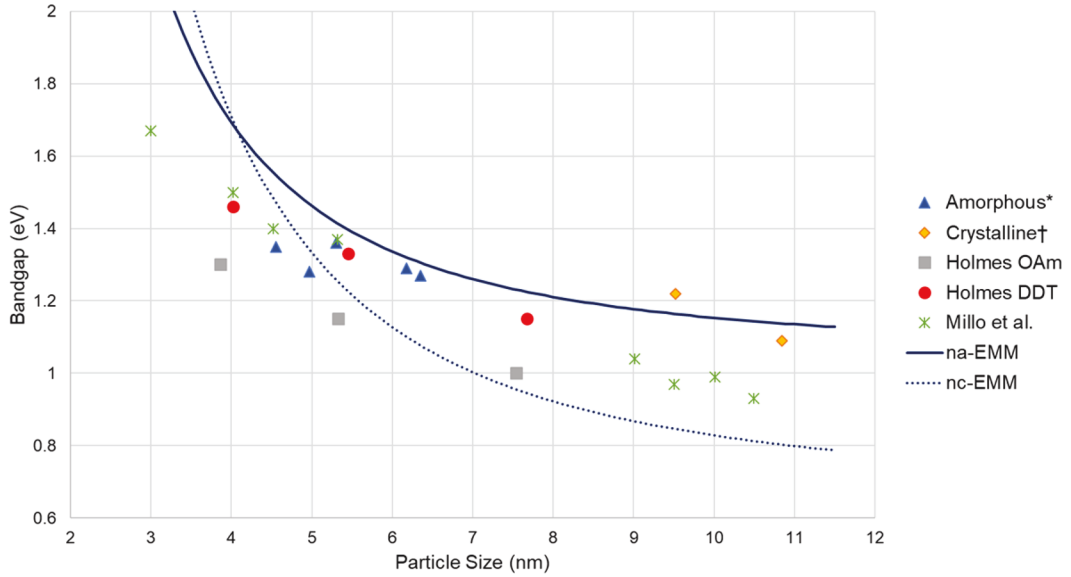

Figure 5. Comparison of optical band gaps with particle size, determined from STEM and TEM measurements. Amorphous and Crystalline entries are from this work. *Amorphous or †Crystalline as determined by PXRD. Holmes OAm, Holmes DDT, and Millo et al. are literature reports where average particle size was determined by TEM.[39,47] na-EMM and nc-EMM are estimates based on the effective mass model.[40]

DOI: 10.1021/acs.inorgchem.8b00334
Inorg. Chem. 2018, 57, 5299−5306

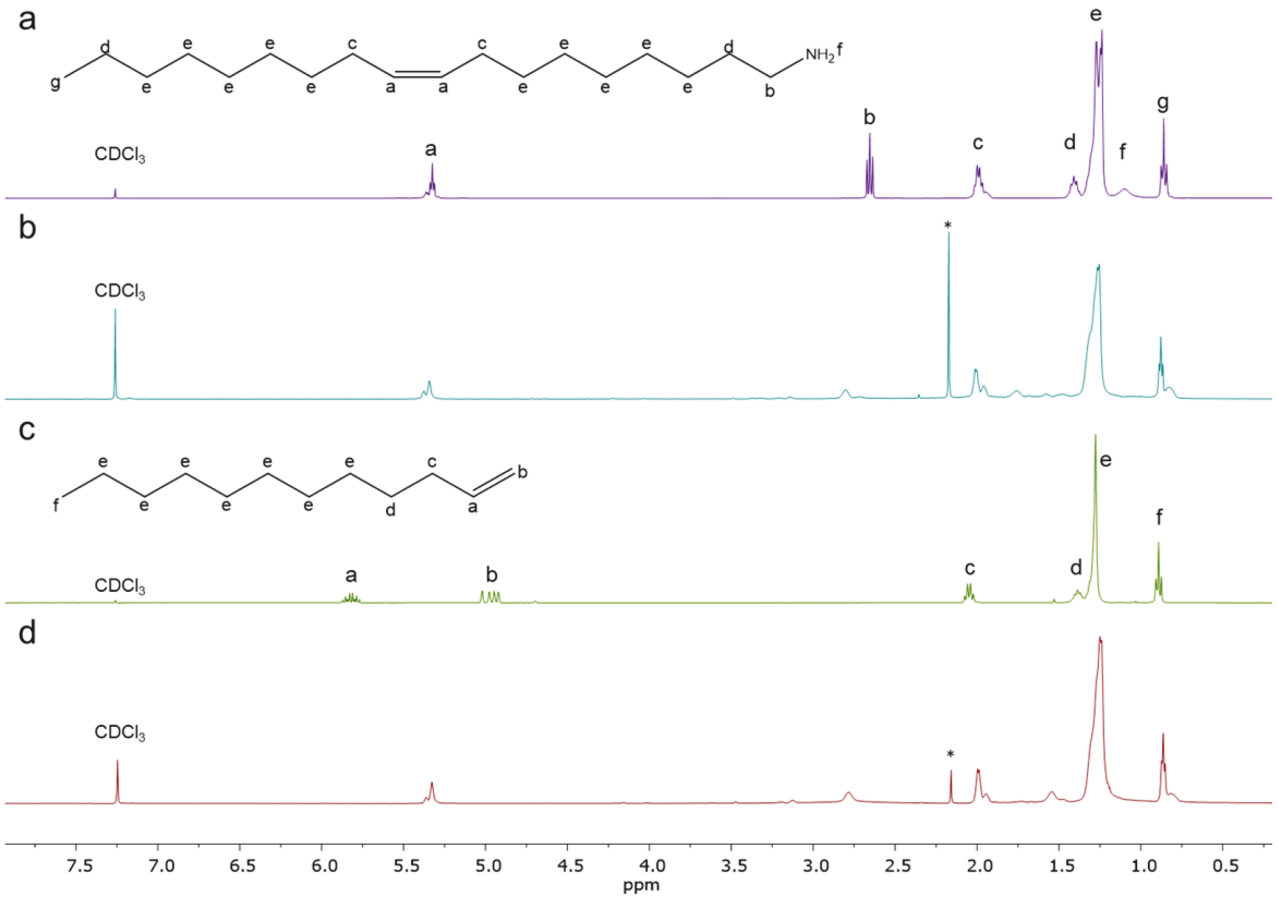

Figure 6. ^{1}H NMR spectra of (a) OAm, (b) Ge NPs made in pure OAm, (c) DDE, and (d) Ge NPs made in 30% DDE. 600 MHz. $CDCl_3$ was used as the solvent for all samples. * Denotes residual methyl toluene peak.

Previous reports of colloidal nanoamorphous Ge have typically been made using milder conditions than that used for producing nanocrystalline Ge. This includes lower temperature or weaker reducing agents such as oleylamine and triethoxysilane.[17,40] Accounts of Ge NPs made in a microwave solution synthesis report crystalline products at temperatures between 210 and 250 °C.[17,39,41] Interestingly, by changing solvent ratios in our system, either crystalline or amorphous Ge NPs can be made at the same temperature, suggesting the ligands on the surface of Ge have a significant impact on crystallinity. These results suggest that surface reconstruction and/or sterics resulting from the differences in bonding of the two organic capping agents to Ge is important.

There is a difference in the manner which the dodecyl and the amine bond to the surface of Ge and the sterics of these two compounds. Additionally, the reducing power of the solvent is changing. Initially, with small amounts of DDE, a slight enlargement of particles is observed via STEM and loss of PXRD occurs. As the reducing power of the solvent is diminished with increasing amounts of DDE, the particle size becomes larger, consistent with a nucleation and growth mechanism.[42] While Ge−N and Ge−C have about the same bond dissociation energy (257 and 255 kJ/mol, respectively), it is known that OAm ligands on Ge NPs synthesized in pure OAm can be easily replaced by a mercaptan.[6] Ge NPs with Ge−C linkages have shown that the Ge−C bond is both kinetically stable to oxidation and resistant to ligand substitution due to its strong covalent character.[43] If both DDE and OAm are bound to the surface, it is possible that the difference in bond lability between the ligands influences disorder on the surface of the Ge NPs. Steric interactions between the tails of the ligands may also influence crystallinity of the NPs. Steric interactions between the ligands would be due to the *cis*-alkene present at the 9th carbon in OAm interacting with the DDE, which is a straight, 12-carbon long hydrocarbon (Chart 1). For the larger NPs, the particles are big enough so that sterics and surface bonding from the ligands may play a significant role in the crystallinity. This may be reflected by the ∼4−5 nm difference between crystallite size and particle size for these NPs. The difference in crystallite size and particles size is much greater for these NPs with OAM and DDE than seen in Ge NPs made in pure OAm for this work (Table 1) and compared to the literature OAm capped Ge NPs.[4,17,39]

Raman spectra of the Ge NPs made with 0%, 40%, and 50% DDE show a sharp peak at 298 cm^{-1} corresponding to the transverse optical mode of crystalline Ge (Figure 3).[44−46] Intermediate concentrations of DDE show a broad peak at 283 cm^{-1} which is consistent with the transverse optical mode of amorphous Ge.[44−46] The Raman spectrum for NPs made in the 5% DDE mixture shows a peak consistent with crystalline Ge, but the peak has broadened toward the amorphous peak considerably, indicating either that the sample consists of a mixture of amorphous and crystalline Ge or that the individual particle has a crystalline and amorphous part. Outside of the 5% DDE NPs, the Raman spectra are consistent with the crystallinity seen in the PXRD.

DOI: 10.1021/acs.inorgchem.8b00334
Inorg. Chem. 2018, 57, 5299−5306

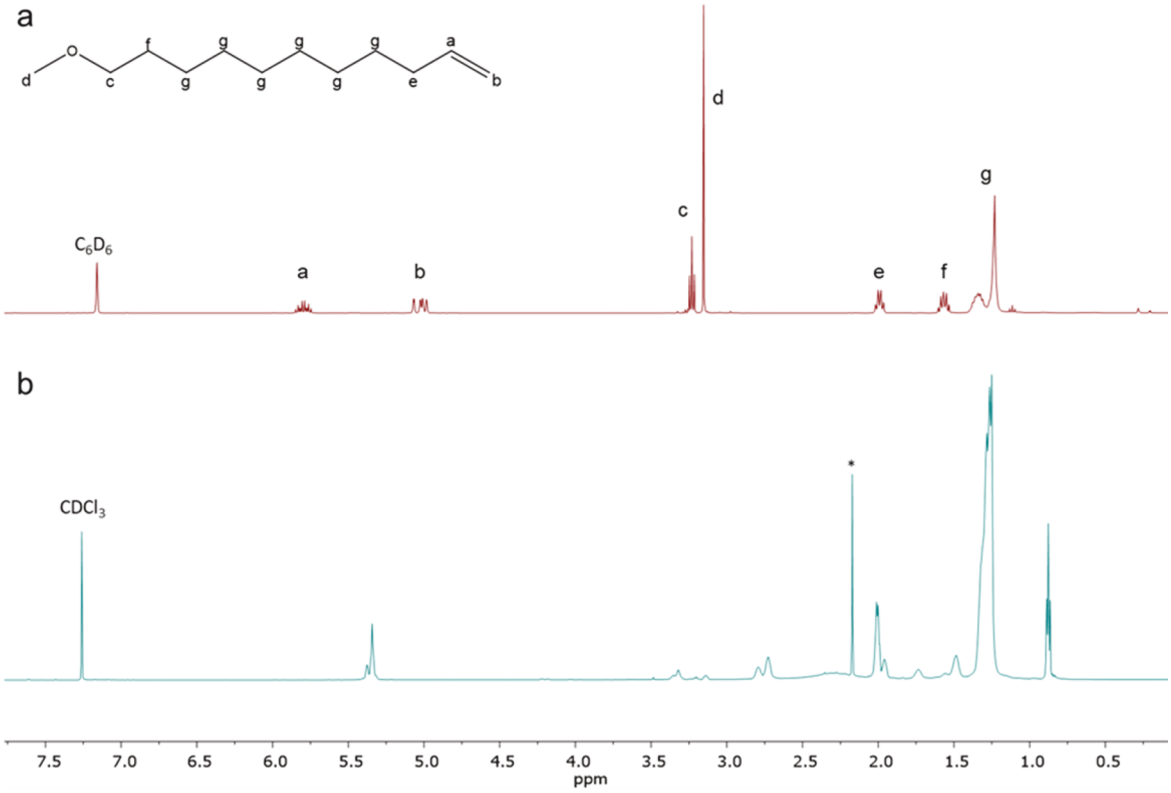

Figure 7. ^{1}H NMR spectra of (a) MUE in C6D6, and (b) Ge NPs made in 10% MUE in CDCL3. 600 MHz. * Denotes residual methyl toluene peak.

FT-IR of the Ge NPs show strong peaks between 2700 and 3000 cm^{-1} corresponding to the alkane C-H stretching and an alkyl C-H bend at 1465 cm^{-1} which stems from the long alkyl chains present in DDE and OAm (Figure 4).[38] The corresponding absorbance spectra are provided in the SI. The samples do not show the DDE C-H alkene stretch at 3075 cm^{-1}, which indicates alkene reduction during the capping reaction. However, Ge NPs made in 0−30% DDE solutions show differences from those made in higher concentrations. Ge NPs made in 0−30% DDE show a weak peak at 3008 cm^{-1} corresponding to the alkene C-H stretch of OAm. As the amount of OAm in the reaction decreases, this weak peak reduces with increasing amounts of DDE and is not visible for the samples prepared with 40−50% DDE. Because this is a weak peak, it is likely that this is a result of dilution rather than loss of the alkene in OAm. This point is further investigated with ^{1}H NMR below. NPs synthesized from 5% to 30% DDE show a broad peak at ∼800 cm^{-1} which is attributed to the N-H bend in OAm. It is possible that this could be a Ge-O stretch as there is some overlap with the Ge-O stretching peak at 800−1000 cm^{-1}. However, GeO_x diffraction peaks are not observed in all of the PXRD of all of those samples, so the assignment to the N-H bend in the high OAm content samples is more consistent. Specific peaks corresponding to Ge-C and Ge-N were not observed with FT-IR.

UV−vis measurements of the Ge NPs were obtained from dilute dispersions of the NPs in toluene in the range of 300−1100 nm. The spectra are featureless and are comparable to previous reports for Ge NPs.[4,17,39,47] Absorption onset was estimated from Tauc plots and values for band gap (E_g) were obtained (SI, Figures S9−S16). E_g was plotted against particle size (from STEM) and compared to previous reports of Ge NPs[4,17,39,47] and the expected values based on the effective mass model (EMM) for crystalline and amorphous Ge NPs[40] (Figure 5). The E_g for the amorphous Ge NPs made here are comparable to previous reports, whereas the E_g for the crystalline Ge NPs were higher than expected. This could be due to the crystalline/amorphous structure of these particles, as the experimental E_g is closer to the theoretical values for amorphous Ge than crystalline Ge.

Compared to the ^{1}H NMR spectrum of molecular OAm (Figure 6a), the Ge-OAm ^{1}H NMR spectrum (Figure 6b; SI, Figure S17) shows peak broadening which is typical for NP ligands.[48] ^{1}H NMR of pure DDE (Figure 6c) and OAm (Figure 6a) have considerable overlap from 1 to 1.5 ppm due to the long hydrocarbon chains present in both molecules. Therefore, Ge NPs made in the DDE−OAm mixtures (Figure 6d) show a similar spectrum to the NPs made in pure OAm. Also present are the α protons to the amine in OAm at 2.70 ppm and OAm's internal alkene protons at 5.4 ppm. While pure DDE has alkene proton peaks at 5.0 and 5.8 ppm, these peaks should not be present in the ^{1}H NMR if the alkene undergoes a hydrogermylation reaction. Because DDE's alkene is reduced to an alkane upon a successful reaction, there is no specific peak in the ^{1}H NMR of the Ge NPs that is diagnostic for DDE. However, if the Ge NPs were only being capped by OAm, the expected peak integration between the hydrocarbon peak at ∼1.27 ppm and the internal alkene from OAm at 5.34 ppm should be a consistent ratio for each sample regardless of DDE concentration. Any change in that peak integration ratio would indicate successful capping of the Ge NPs with some amount of dodecyl. ^{1}H NMR of both the solvent OAm and Ge NPs made with OAm shows that the alkene:hydrocarbon proton ratio is 1:13.3. For Ge NPs made in 5% DDE, that ratio increased to

DOI: 10.1021/acs.inorgchem.8b00334
Inorg. Chem. 2018, 57, 5299−5306

1:16.4, which indicates the presence of extra hydrocarbons not accounted for in OAm. The ratio steadily increased as the DDE concentration was increased, reaching a peak of 1:19.6 for the Ge NPs made in 50% DDE. While the peak integration ratios are supportive of the hypothesis that the Ge NPs have some amount of dodecyl bound to the NP surface (if it was only associated, the vinylic protons of DDE would still be present), a specific diagnostic peak for a comparable ligand was strongly desired to definitively prove the alkyl was bound to the surface. For this reason, MUE was synthesized as a replacement ligand for DDE in the reaction.

MUE was chosen as a replacement for DDE because it has the same terminal alkene as DDE but also contains a methoxy group at the end of the carbon chain that adds a sharp singlet at around 3.2 ppm in its ^{1}H NMR which can be used as a diagnostic peak (Figure 7a). MUE was successfully synthesized from 11-bromo-1-undecene via a Williamson ether synthesis. Ge NPs were synthesized in 5% and 10% mixtures of MUE with OAm. The Ge NPs produced were amorphous by PXRD, like those produced with the same percentage of DDE. ^{1}H NMR of the Ge NPs made in the 10% MUE−OAm mixtures show both the diagnostic peaks for MUE and OAm (Figure 7b). Of note, the alkene peak in MUE disappears as expected, which indicates that the alkene is reduced during the reaction and therefore presumably bound to the NP surface and not associated with the OAm ligands attached to the Ge NP surface. The surface ligand ratio for the Ge NPs can be determined by integrating the diagnostic peaks in the ^{1}H NMR. Integration of the ^{1}H NMR obtained from the Ge NPs made in the 10% MUE−OAm mixture gives a ratio of 1:5.68 MUE:OAm, indicating that 17% of the Ge NP ligands are MUE.

CONCLUSION

Ge NPs were successfully made via a microwave-assisted synthesis using a solvent mixture of oleylamine and 1-dodecene without employing *n*- or *tert*-BuLi or another strong reducing agent. TEM and PXRD showed that increasing the amount of DDE in the reaction generally increased the NP diameter. PXRD and Raman spectroscopy also showed that NPs made at lower concentrations (<40%) of DDE were amorphous, whereas NPs made at higher concentrations were crystalline, supported by PXRD and lattice fringes in STEM. The lack of crystallinity for the lower concentrations of DDE was attributed to both steric effects and the different surface bonding of the amine and alkyl ligands. ^{1}H NMR of Ge NPs synthesized in a mixture of oleylamine and 11-methoxyundec-1-ene conclusively shows that both molecules act as ligands in this system. ^{1}H NMR also shows the loss of DDE and MUE's alkene protons after the reaction, which indicates that the alkene is reduced via a hydrogermylation route to form the Ge−C bond.

ASSOCIATED CONTENT

Supporting Information

The Supporting Information is available free of charge on the ACS Publications website at DOI: 10.1021/acs.inorgchem.8b00334.

STEM images and histograms of the Ge NPs, Tauc plots generated from the UV−vis data, ^{1}H NMR of the Ge NPs, and FT-IR of the Ge NPs plotted in absorbance mode (PDF)

AUTHOR INFORMATION

Corresponding Author

*E-mail: smkauzlarich@ucdavis.edu.

ORCID

Andrew Bernard: 0000-0002-3673-2938

Susan M. Kauzlarich: 0000-0002-3627-237X

Author Contributions

†These authors contributed equally. The manuscript was written through contributions of all authors. All authors have given approval to the final version of the manuscript.

Notes

The authors declare no competing financial interest.

ACKNOWLEDGMENTS

Financial support from the National Science Foundation (CHE-1710110) is gratefully acknowledged. We thank R. Blair (University of South Florida) for providing phase-pure Ge(II) iodide. We also thank the University of California, Davis NEAT ORU Keck Spectral Imaging Facility for the use of their laser Raman microscope.

REFERENCES

(1) Church, C. P.; Muthuswamy, E.; Zhai, G.; Kauzlarich, S. M.; Carter, S. A. Quantum Dot Ge/TiO_2 Heterojunction Photoconductor Fabrication and Performance. *Appl. Phys. Lett.* **2013**, *103*, 223506.

(2) Liang, W.; Yang, H.; Fan, F.; Liu, Y.; Liu, X. H.; Huang, J. Y.; Zhu, T.; Zhang, S. Tough Germanium Nanoparticles under Electrochemical Cycling. *ACS Nano* **2013**, *7*, 3427−3433.

(3) Michalet, X.; Pinaud, F. F.; Bentolila, L. A.; Tsay, J. M.; Doose, S.; Li, J. J.; Sundaresan, G.; Wu, A. M.; Gambhir, S. S.; Weiss, S. Quantum Dots for Live Cells, in Vivo Imaging, and Diagnostics. *Science* **2005**, *307*, 538−544.

(4) Ruddy, D. A.; Johnson, J. C.; Smith, E. R.; Neale, N. R. Size and Bandgap Control in the Solution-Phase Synthesis of near-Infrared-Emitting Germanium Nanocrystals. *ACS Nano* **2010**, *4*, 7459−7466.

(5) Wu, S.; Han, C.; Iocozzia, J.; Lu, M.; Ge, R.; Xu, R.; Lin, Z. Germanium-Based Nanomaterials for Rechargeable Batteries. *Angew. Chem., Int. Ed.* **2016**, *55*, 7898−7922.

(6) Muthuswamy, E.; Zhao, J.; Tabatabaei, K.; Amador, M. M.; Holmes, M. A.; Osterloh, F. E.; Kauzlarich, S. M. Thiol-Capped Germanium Nanocrystals: Preparation and Evidence for Quantum Size Effects. *Chem. Mater.* **2014**, *26*, 2138−2146.

(7) Purkait, T. K.; Swarnakar, A. K.; De Los Reyes, G. B.; Hegmann, F. A.; Rivard, E.; Veinot, J. G. One-Pot Synthesis of Functionalized Germanium Nanocrystals from a Single Source Precursor. *Nanoscale* **2015**, *7*, 2241−2244.

(8) Tanke, R. S.; Kauzlarich, S. M.; Patten, T. E.; Pettigrew, K. A.; Murphy, D. L.; Thompson, M. E.; Lee, H. W. H. Synthesis of Germanium Nanoclusters with Irreversibly Attached Functional Groups: Acetals, Alcohols, Esters, and Polymers. *Chem. Mater.* **2003**, *15*, 1682−1689.

(9) Ma, X.; Wu, F.; Kauzlarich, S. M. Alkyl-Terminated Crystalline Ge Nanoparticles Prepared from Nage: Synthesis, Functionalization and Optical Properties. *J. Solid State Chem.* **2008**, *181*, 1628−1633.

(10) Taylor, B. R.; Kauzlarich, S. M.; Delgado, G. R.; Lee, H. W. H. Solution Synthesis and Characterization of Quantum Confined Ge Nanoparticles. *Chem. Mater.* **1999**, *11*, 2493−2500.

(11) Taylor, B. R.; Kauzlarich, S. M.; Lee, H. W. H.; Delgado, G. R. Solution Synthesis of Germanium Nanocrystals Demonstrating Quantum Confinement. *Chem. Mater.* **1998**, *10*, 22−24.

(12) Lee, H.; Kim, M. G.; Choi, C. H.; Sun, Y.-K.; Yoon, C. S.; Cho, J. Surface-Stabilized Amorphous Germanium Nanoparticles for Lithium-Storage Material. *J. Phys. Chem. B* **2005**, *109*, 20719−20723.

(13) Chiu, H. W.; Chervin, C. N.; Kauzlarich, S. M. Phase Changes in Ge Nanoparticles. *Chem. Mater.* **2005**, *17*, 4858−4864.

DOI: 10.1021/acs.inorgchem.8b00334
Inorg. Chem. 2018, 57, 5299−5306

(14) Lu, X.; Korgel, B. A.; Johnston, K. P. High Yield of Germanium Nanocrystals Synthesized from Germanium Diiodide in Solution. *Chem. Mater.* **2005**, *17*, 6479−6485.
(15) Jing, C.; Zang, X.; Bai, W.; Chu, J.; Liu, A. Aqueous Germanate Ion Solution Promoted Synthesis of Worm-Like Crystallized Ge Nanostructures under Ambient Conditions. *Nanotechnology* **2009**, *20*, 505607.
(16) Wu, J.; Sun, Y.; Zou, R.; Song, G.; Chen, Z.; Wang, C.; Hu, J. One-Step Aqueous Solution Synthesis of Ge Nanocrystals from Geo2 Powders. *CrystEngComm* **2011**, *13*, 3674−3677.
(17) Muthuswamy, E.; Iskandar, A. S.; Amador, M. M.; Kauzlarich, S. M. Facile Synthesis of Germanium Nanoparticles with Size Control: Microwave Versus Conventional Heating. *Chem. Mater.* **2013**, *25*, 1416−1422.
(18) Lu, X.; Ziegler, K. J.; Ghezelbash, A.; Johnston, K. P.; Korgel, B. A. Synthesis of Germanium Nanocrystals in High Temperature Supercritical Fluid Solvents. *Nano Lett.* **2004**, *4*, 969−974.
(19) Vaughn, D. D., 2nd; Schaak, R. E. Synthesis, Properties and Applications of Colloidal Germanium and Germanium-Based Nanomaterials. *Chem. Soc. Rev.* **2013**, *42*, 2861−2879.
(20) Chiu, H. W.; Kauzlarich, S. M.; Sutter, E. Thermal Behavior and Film Formation from an Organogermanium Polymer/Nanoparticle Precursor. *Langmuir* **2006**, *22*, 5455−5458.
(21) Toko, K.; Nakao, I.; Sadoh, T.; Noguchi, T.; Miyao, M. Electrical Properties of Poly-Ge on Glass Substrate Grown by Two-Step Solid-Phase Crystallization. *Solid-State Electron.* **2009**, *53*, 1159−1164.
(22) Carolan, D.; Doyle, H. Size Controlled Synthesis of Germanium Nanocrystals: Effect of Ge Precursor and Hydride Reducing Agent. *J. Nanomater.* **2015**, *2015*, 506056.
(23) Kennedy, T.; Mullane, E.; Geaney, H.; Osiak, M.; O'Dwyer, C.; Ryan, K. M. High-Performance Germanium Nanowire-Based Lithium-Ion Battery Anodes Extending over 1000 Cycles through in Situ Formation of a Continuous Porous Network. *Nano Lett.* **2014**, *14*, 716−723.
(24) Wu, J.; Han, L.; Wang, N.; Song, Y.; Chen, H.; Chen, H.; Hu, J. In Situ Structural Evolution from Geo Nanospheres to Geo/(Ge, Geo2) Core-Shell Nanospheres and to Ge Hollow Nanospheres. *CrystEngComm* **2011**, *13*, 4611−4616.
(25) Li, L.; Seng, K. H.; Feng, C.; Liu, H. K.; Guo, Z. Synthesis of Hollow Geo2 Nanostructures, Transformation into Ge@C, and Lithium Storage Properties. *J. Mater. Chem. A* **2013**, *1*, 7666−7672.
(26) Carolan, D.; Doyle, H. Efficient One-Pot Synthesis of Monodisperse Alkyl-Terminated Colloidal Germanium Nanocrystals. *J. Nanopart. Res.* **2014**, *16*, 2721.
(27) Lee, D. C.; Pietryga, J. M.; Robel, I.; Werder, D. J.; Schaller, R. D.; Klimov, V. I. Colloidal Synthesis of Infrared-Emitting Germanium Nanocrystals. *J. Am. Chem. Soc.* **2009**, *131*, 3436−3437.
(28) Fan, J.; Chu, P. K. Group Iv Nanoparticles: Synthesis, Properties, and Biological Applications. *Small* **2010**, *6*, 2080−2098.
(29) Reiss, P.; Carriere, M.; Lincheneau, C.; Vaure, L.; Tamang, S. Synthesis of Semiconductor Nanocrystals, Focusing on Nontoxic and Earth-Abundant Materials. *Chem. Rev.* **2016**, *116*, 10731−10819.
(30) Nakamura, Y.; Watanabe, K.; Fukuzawa, Y.; Ichikawa, M. Observation of the Quantum-Confinement Effect in Individual Ge Nanocrystals on Oxidized Si Substrates Using Scanning Tunneling Spectroscopy. *Appl. Phys. Lett.* **2005**, *87*, 133119.
(31) Takeoka, S.; Fujii, M.; Hayashi, S.; Yamamoto, K. Size-Dependent near-Infrared Photoluminescence from Ge Nanocrystals Embedded in Sio2Matrices. *Phys. Rev. B: Condens. Matter Mater. Phys.* **1998**, *58*, 7921−7925.
(32) Choi, K.; Buriak, J. M. Hydrogermylation of Alkenes and Alkynes on Hydride-Terminated Ge(100) Surfaces. *Langmuir* **2000**, *16*, 7737−7741.
(33) Song, L.; Yan, C.; Zhang, W.; Wu, H.; Jia, Z.; Ma, M.; Xie, J.; Gu, N.; Zhang, Y. Influence of Reaction Solvent on Crystallinity and Magnetic Properties of Mnfe2o4 Nanoparticles Synthesized by Thermal Decomposition. *J. Nanomater.* **2016**, *2016*, 4878935.
(34) Zimdars, J.; Bredol, M. On the Influence of Coordinating Solvents on the Reduction of Selenium for the Phosphine-Free Synthesis of Metal Selenide Nanoparticles. *New J. Chem.* **2016**, *40*, 1137−1142.
(35) Costanzo, S.; Simon, G.; Richardi, J.; Colomban, P.; Lisiecki, I. Solvent Effects on Cobalt Nanocrystal Synthesis—a Facile Strategy to Control the Size of Co Nanocrystals. *J. Phys. Chem. C* **2016**, *120*, 22054−22061.
(36) Restrepo, D. T.; Lynch, K. E.; Giesler, K.; Kuebler, S. M.; Blair, R. G. Low-Temperature (210°C) Deposition of Crystalline Germanium Via in Situ Disproportionation of Gei2. *Mater. Res. Bull.* **2012**, *47*, 3484−3488.
(37) Faig, A.; Petersen, L. K.; Moghe, P. V.; Uhrich, K. E. Impact of Hydrophobic Chain Composition on Amphiphilic Macromolecule Antiatherogenic Bioactivity. *Biomacromolecules* **2014**, *15*, 3328−3337.
(38) Mourdikoudis, S.; Liz-Marzán, L. M. Oleylamine in Nanoparticle Synthesis. *Chem. Mater.* **2013**, *25*, 1465−1476.
(39) Holmes, A. L.; Hütges, J.; Reckmann, A.; Muthuswamy, E.; Meerholz, K.; Kauzlarich, S. M. Probing Electronics as a Function of Size and Surface of Colloidal Germanium Nanocrystals. *J. Phys. Chem. C* **2015**, *119*, 5671−5678.
(40) Dag, Ö.; Henderson, E. J.; Ozin, G. A. Synthesis of Nanoamorphous Germanium and Its Transformation to Nanocrystalline Germanium. *Small* **2012**, *8*, 921−929.
(41) Tabatabaei, K.; Lu, H.; Nolan, B. M.; Cen, X.; McCold, C. E.; Zhang, X.; Brutchey, R. L.; van Benthem, K.; Hihath, J.; Kauzlarich, S. M. Bismuth Doping of Germanium Nanocrystals through Colloidal Chemistry. *Chem. Mater.* **2017**, *29*, 7353−7363.
(42) Donegá, C. d. M.; Liljeroth, P.; Vanmaekelbergh, D. Physicochemical Evaluation of the Hot-Injection Method, a Synthesis Route for Monodisperse Nanocrystals. *Small* **2005**, *1*, 1152−1162.
(43) Ruddy, D. A. E.; Peter, T.; Habas, S. E.; Seabold, J. A.; Neale, N. R. Surface Chemistry Exchange of Alloyed Germanium Nanocrystals: A Pathway toward Conductive Group Iv Nanocrystal Films. *J. Phys. Chem. Lett.* **2013**, *4*, 416−421.
(44) Yashiki, Y.; Miyajima, S.; Yamada, A.; Konagai, M. Preparation of Microcrystalline Germanium Carbon Thin Films by Hot-Wire Chemical Vapor Deposition Using Dimethylgermane. *Jpn. J. Appl. Phys.* **2007**, *46*, 2865.
(45) Chang, J. E.; Liao, P. H.; Chien, C. Y.; Hsu, J. C.; Hung, M. T.; Chang, H. T.; Lee, S. W.; Chen, W. Y.; Hsu, T. M.; George, T.; Li, P. W. Matrix and Quantum Confinement Effects on Optical and Thermal Properties of Ge Quantum Dots. *J. Phys. D: Appl. Phys.* **2012**, *45*, 105303.
(46) Benzi, P.; Bottizzo, E.; Demaria, C.; Infante, G.; Iucci, G.; Polzonetti, G. Amorphous Nonstoichiometric Ge1−X−Cx:H Compounds Obtained by Radiolysis-Chemical Vapor Deposition of Germane/Ethyne or Germane/Allene Systems: A Bonding and Microstructure Investigation Performed by X-Ray Photoelectron Spectroscopy and Raman Spectroscopy. *J. Appl. Phys.* **2007**, *101*, 124906.
(47) Millo, O.; Balberg, I.; Azulay, D.; Purkait, T. K.; Swarnakar, A. K.; Rivard, E.; Veinot, J. G. C. Direct Evaluation of the Quantum Confinement Effect in Single Isolated Ge Nanocrystals. *J. Phys. Chem. Lett.* **2015**, *6*, 3396−3402.
(48) Marbella, L. E.; Millstone, J. E. NMR Techniques for Noble Metal Nanoparticles. *Chem. Mater.* **2015**, *27*, 2721−2739.

DOI: 10.1021/acs.inorgchem.8b00334
Inorg. Chem. 2018, 57, 5299−5306